ACS APPLIED POLYMER MATERIALS

pubs.acs.org/acsapm Article

Effect of Molecular Weight and Layer Thickness on the Dielectric Breakdown Strength of Neat and Homopolymer Swollen Lamellar Block Copolymer Films

Saumil Samant, Monali Basutkar, Maninderjeet Singh, Ali Masud, Christopher A. Grabowski, Kim Kisslinger, Joseph Strzalka, Guangcui Yuan, Sushil Satija, Ikeoluwa Apata, Dharmaraj Raghavan, Michael Durstock, and Alamgir Karim*

Cite This: *ACS Appl. Polym. Mater.* 2020, 2, 3072−3083 Read Online

ACCESS | Metrics & More | Article Recommendations | Supporting Information

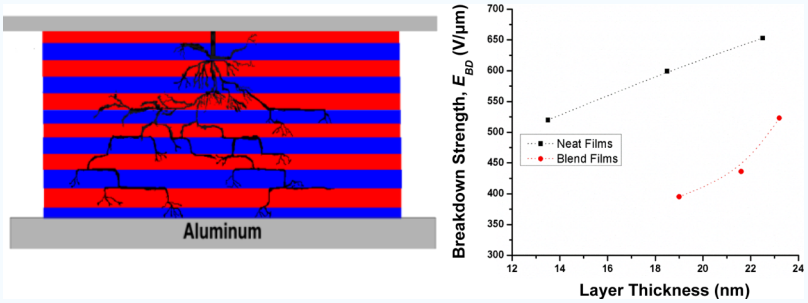

ABSTRACT: Designing next-generation lightweight pulsed power devices hinges on understanding the factors influencing the energy storage performance of dielectric materials. Polymer dielectric films have a quadratic dependence of energy storage on the voltage breakdown strength, and strategies to enhance the breakdown strength are expected to yield a path toward high energy storage densities. Highly stratified lamellar block copolymer (L-BCP) films of model polystyrene-*b*-polymethylmethacrylate (PS-*b*-PMMA) exhibited as much as ∼50% enhancement in breakdown voltage (E_{BD}) (225% increase in stored energy density, $U \sim E_{BD}^2$) compared to unordered as-cast L-BCP films. Such an energy density using amorphous polymer is on par with industry-standard semicrystalline biaxially oriented polypropylene (BOPP) and as such a notable development in the field. This work develops a deeper understanding of the molecular mechanisms of E_{BD} enhancement in L-BCP films, relating E_{BD} directly to molecular weight (M_n), with interpretation to effects of chain-end density and distribution, interface formation, layer thickness, and their relative contributions. As-cast disordered L-BCP films show decreasing E_{BD} with decreasing M_n similar to homopolymer studies because of the increase of homogeneously distributed chain ends in the film. E_{BD} increases significantly in parallel ordered L-BCP films because of the combination of interface formation and spatial isolation of the chain ends into segregated zones. We further confirm the role of chain ends in the breakdown process blending a low M_n L-BCP with matched M_n homopolymers to attain the same layer spacing as neat L-BCP of higher M_n. E_{BD} shows a significant decrease at low homopolymer fractions because of increased net chain-end density within swollen ordered L-BCP domains in wet-brush regime, followed by increased E_{BD} because of layer thickness increase via segregated "interphase layer" formation by excess homopolymers. Notably, E_{BD} of homopolymer swollen L-BCPs is always lower than that of neat L-BCPs of the same domain spacing because of overall adverse chain-end contribution from homopolymers. These findings provide important selection rules for L-BCPs for designing next-generation flexible electronics with high energy density solid-state BCP film capacitors.

KEYWORDS: *electrostatic capacitors, polymer capacitor, dielectric, barrier effect, breakdown strength, block copolymers, directed self-assembly, cold zone annealing-soft shear*

INTRODUCTION

Polymer films are widely used as the dielectric material in capacitors because of their flexibility, processability, and higher operating voltages as compared to alternative ceramic insulators. However, the energy density of current polymer capacitors falls significantly short of the rising demands for high-power film capacitors for advanced applications such as

Received: March 3, 2020
Accepted: June 30, 2020
Published: June 30, 2020

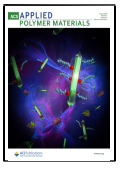

https://dx.doi.org/10.1021/acsapm.0c00127
ACS Appl. Polym. Mater. 2020, 2, 3072−3083

electric vehicles, pulsed lasers, aviation, and flexible electronics. The maximum energy density (U) that can be stored within a capacitor is expressed as

$$U = \frac{1}{2}\varepsilon_0\varepsilon_r {E_{BD}}^2 \quad (1)$$

where ε_r is the dielectric permittivity, E_{BD} is the breakdown strength of the dielectric material, and ε_0 is the permittivity of free space.

Although significant efforts have been made to increase the ε_r of polymer film capacitors using nanocomposites or nanodielectrics,[1−6] enhancement of E_{BD} of polymeric materials without the use of fillers has not received significant attention. As expressed in eq 1, the energy density has a quadratic dependence on E_{BD} and thus enhancement of E_{BD} holds greater significance for improving the current energy densities of polymer-based capacitors.

In polymers, dielectric breakdown is traditionally assumed to occur by an electron avalanche mechanism which leads to the formation of fractal electrical trees across the material.[7,8] These electrical trees are facilitated by structural defects in the material and propagate toward the electrodes. Increasing the breakdown strength requires inhibition of the propagation of these trees. Vogelsang et al.[9] demonstrated through simulations that the presence of barriers within dielectric material can provide a tortuous pathway to the treeing, resulting in breakdown inhibition. Especially, the presence of a permittivity or conductivity contrast between adjacent layers of the dielectric and barrier leads to the formation of space charge at the interface which redistributes the applied electric field, forestalling the breakdown process, thus enhancing the overall dielectric strength. Experimentally, Wolak et al.[10] imaged the damage caused by an electrical breakdown in a homogeneous film versus a multilayer coextruded film using a sequential focused ion beam (FIB)−scanning electron microscopy procedure. In homogeneous films, the damage was confined to the small volume at the pinhole site, whereas for alternating polycarbonate/poly(vinylidenefluoride-hexafluoropropylene) (PC/P[VDF-HFP]) multilayer films, the damaged zone extended laterally up to 15 μm into the film along the layer interfaces indicating a tortuous pathway to the treeing, resulting in breakdown inhibition. The energy densities of structured multilayered polymer films obtained using forced-assembly multilayer coextrusion were found to be about 60% greater than that of the pure component polymers. Despite the forced assembly coextrusion method showing improvements in energy densities over pure components, several shortcomings such as nonuniform layer widths, large defects, voids, and layer delamination can limit the performance of coextruded multilayer films. Additionally, the coextrusion process can limit the orientation of the layers and the type of polymer components that can be layered because of adhesion constraints.

Recently, we demonstrated a new material design and processing strategy for the fabrication of multilayered, multicomponent, barrier dielectric films using directed self-assembly (DSA) of lamellar block copolymer (L-BCP) films, with the lamellae aligned parallel to the substrate electrode or normal to the applied electric field. Essentially, a high degree of ordering and orientation control of the microdomains along with tunability of dielectric contrast, layer thickness, and interfacial width could be achieved using DSA techniques applied to these L-BCP films. The application of DSA via cold zone annealing-soft shear (CZA-SS)[39−41] to polystyrene-*b*-polymethylmethacrylate (PS-*b*-PMMA) L-BCP films revealed a ≈20−50% enhancement in E_{BD} translating to a ≈225% increase in theoretical energy density U for the self-assembled multilayer BCP films compared to unordered single-phase as-cast films, suggesting that the breakdown pathway is highly selective to the polymer nanostructure within the limited molecular weight range of BCP studied.[11] The improvement in E_{BD} was attributed to the presence of multiple PS/PMMA interfacial barriers within the multilayered BCP dielectric film that forestall electrical treeing propagation during the breakdown.

In order to further improve the capacitor performance of highly ordered lamellar block copolymer films, it is imperative to study the factors that can affect the breakdown strength of self-assembled block copolymer films. Reports in the literature have demonstrated that the breakdown strength of homopolymer films increases with an increase in molecular weight, citing a lower number of chain ends per unit volume (chain-end density, ρ_c) or higher regularity of the chain structure (chain-end distribution) in high molecular weight polymers as possible explanations.[12−14] In terms of multilayered films, earlier studies have reported that the breakdown strength of coextruded films can be influenced by the type of polymer, individual layer thickness as well as the number of layers within the film.[15−20] Zhou et al.[21] studied the layer thickness effect in coextruded multilayered PC/coPVDF films and found that an optimal layer thickness of ≈160 nm corresponding to about 65 layers in a 10 μm film gave the highest dielectric lifetime under a breakdown field of 320 kV/mm. However, detailed studies of effects of individual block layer thicknesses, the total number of layers, or the molecular weight of BCP on E_{BD} of BCP dielectric films have not been performed. Thus, the objective of the present study was to evaluate the influence of layer thickness, molecular weight, and associated factors, such as chain-end density and distribution and nature of the dielectric interface defined by the L-BCP junction plane, on the dielectric properties of the BCP film.

However, for BCP systems there exists a direct correlation between molecular weight and layer thickness. In the weak segregation limit (as is the case for the BCPs in this study), the domain size L_0 ($2d$) scales as[22,42,43]

$$L_0 \propto N^{0.5} \quad (2)$$

where N is the degree of polymerization, which is a direct measure of the molecular weight, M_n. For PS-*b*-PMMA, the domain size scales as ${M_n}^{0.5}$. Any increase in molecular weight also translates to an increase in domain size and the effective layer thickness for a constant film thickness. Therefore, to study the effects of molecular weight and layer thickness independently on the dielectric properties of the BCP, it is necessary to decouple the molecular weight and layer thickness parameters. This can be potentially achieved by tuning the domain sizes of the BCP (increasing layer thickness) without affecting the molecular weight. To that end, PS-*b*-PMMA BCP were blended with component PS and PMMA homopolymers having comparable molecular weight to selectively swell the BCP domains, thereby increasing layer thickness but maintaining the overall molecular weight of the system. BCP-homopolymer ternary blends have been extensively studied in the literature with respect to composition, phase separation, and expected morphologies.[42] Russell et al. have studied the distribution of homopolymers with varying

https://dx.doi.org/10.1021/acsapm.0c00127
ACS Appl. Polym. Mater. 2020, 2, 3072−3083

molecular weights in parallel ordered BCPs using neutron reflectivity (NR).[29] They reported that if the molecular weights of the added homopolymers are considerably lower as compared to the BCP, then the homopolymer chains uniformly solubilize within the BCP domains. A similar phenomenon was observed by Ryu et al. while studying the temperature dependence of the domain size of BCP swollen with homopolymers.[32] Torikai et al. have quantified the domain sizes of BCP having a uniform distribution of homopolymers[23]

$$L = L_0(1 - \varphi_H)^{-1/3} \quad (3)$$

where L and L_0 are the lamellar domain size of the blend and neat BCP, respectively, and φ_H is the total volume fraction of added homopolymers. If the molecular weights of the homopolymers are comparable to those of individual blocks of the BCP as is the case with this study, the blended homopolymer components localize at the center of the respective domains and swell the individual blocks along the direction normal to the interface with a stronger dependence of domain size (L_0) on added volume fraction of homopolymer (φ_H), theoretically computed[23] as

$$L = L_0(1 - \varphi_H)^{-1} \quad (4)$$

The localization is related to the translational and configurational entropy of the homopolymer chains within the blocks.[24]

We examined these ternary blend films with an equal concentration of PS and PMMA homopolymers in PS-*b*-PMMA to ensure symmetric swelling of the individual PS and PMMA layers within the film. This approach is expected to increase the domain size or individual layer thickness of the L-BCP while maintaining the lamellar morphology of the BCP up to the Lifshitz concentration point of the system with increasing added homopolymer volume fraction (φ_H). Through the present study, we establish that E_{BD} increased nearly linearly with an increase of molecular weight in as-cast, largely unordered PS-*b*-PMMA L-BCP films, as well as in ordered L-BCP films. In the unordered as-cast films, chain ends which act as defect sites for breakdown within the films are homogeneously distributed and the increase of E_{BD} with M_n in as-cast films is attributed to decreased chain ends (defect sites) per unit volume. This is similar to E_{BD} variation with M_n in homopolymer films, clearly attributed to chain-end density variation. However, in ordered L-BCP films, the jump-increase in E_{BD} is effected by a combination of sharp PS−PMMA interface and PS/PMMA layer formation as well as inhomogeneous (segregated) distribution of chains ends within the films. As defined in multilayer extrusion terms, the "layer" thickness $d = L_0/2$,[30,31] where L_0 is the L-BCP domain spacing. Specifically, with increasing molecular weight of the L-BCP, not only is there a reduction of chain-end density, there is an increase of layer thickness. Notably, interfacial width is set by χ which also presumably plays a role in controlling E_{BD}. However, χ is fixed for the PS−PMMA system, so the interfacial width should be invariant with change of M_n to first order.

By comparison, ordered ternary blend films of added matched molecular weight homopolymers to L-BCP exhibit an initial drastic decrease of E_{BD} at low volume fraction of added homopolymers, followed by a progressive increase of E_{BD} at higher concentrations. The L-BCP chosen in the ternary blend system is the lowest 19.1k−18.5k PS-*b*-PMMA, so that by adding the dual homopolymers, its layer thickness can be increased to match that of a higher M_n L-BCP and compared to its E_{BD}. In this way, any difference in E_{BD} can be attributed to factors other than layer thickness. Overall, ternary blends always show lower absolute values of E_{BD} compared to neat L-BCP with matched domain spacing/layer thickness. The initial decrease of E_{BD} in ternary blends can be attributed to solubilization of homopolymers by the L-BCP "brushes" at low homopolymer concentration that does not lead to much layer thickness increase. Rather increased homogenous distribution of added homopolymer chain ends results in the decrease of E_{BD}. At higher homopolymer concentration however, the L-BCP "brush" layers get saturated with solubilized homopolymers, and a localization-driven "interphase" formation process results in layer thickness leading to the increase of E_{BD}. Even so, the increase is very modest, as chain-end density in the overall layer is increasing with the increase of homopolymer volume fraction. Such L-BCP solubilization of homopolymers at low concentration, followed by their localization at higher concentration, has been reported in another similar ternary system.[42] In summary, these findings can have a major bearing in strategies for improving the breakdown strength of L-BCP-based polymer film capacitors, for designing next-generation high energy density polymer dielectrics for energy storage.

EXPERIMENTAL SECTION

Materials. The effect of a self-assembled multilayered lamellar structure on the breakdown properties was studied using the model lamellae forming BCP system PS-*b*-PMMA, where the individual blocks have disparate dielectric breakdown values (PS ≈ 250 V/μm, PMMA ≈ 500 V/μm), but relatively close dielectric permittivity at 1 kHz [PS ($\varepsilon_r \approx 2.6$), PMMA ($\varepsilon_r \approx 3.2$)]. For this study, PS-*b*-PMMA with molecular weights 19.5-*b*-18.1 (37.6 kg mol^{-1}), 33-*b*-33 (66 kg mol^{-1}), and 45-*b*-44 (89 kg mol^{-1}) and homopolymers PS (14 kg mol^{-1}) and PMMA (16 kg mol^{-1}) were purchased from Polymer Source Inc. and used as received. Deuterated dPS-*b*-PMMA (19.5-*b*-18.1) (37.6 kg/mol) purchased from Polymer Source Inc. was used for the NR studies to enhance the neutron contrast between layers. Quartz slides (75 mm × 25 mm × 1 mm) purchased from GM Associates Inc. were used as the substrates for all the experiments.

Film Preparation. Prior to film casting on the slides, electron beam physical vapor deposition was utilized to coat 100 nm thick aluminum films (roughness ≈ 2 nm) onto quartz slides to form the bottom electrode for breakdown testing. Polymer solutions (a mass fraction of 10%) were prepared by dissolving in toluene. Measured amounts of PS (14 kg mol^{-1}) and PMMA (16 kg mol^{-1}) homopolymer solutions were added to the PS-*b*-PMMA (19.5-*b*-18.1 kg mol^{-1}) solution to prepare blend solutions with mass fractions (φ_H) of 20, 40, and 60% with respect to the BCP. The higher molecular weight and blend solutions were flow-coated on to UV−ozone (Novoscan Tech., Inc.) cleaned Al-coated (1 in. × 3 in.) quartz slides to achieve uniform films with thicknesses of ≈1 μm. The thicknesses of the casted film were measured using a Bruker DektakXT profilometer. Prior to processing, the films were dried in a vacuum oven at 65 °C for 12 h to remove the residual solvent in the casted film.

CZA-SS Processing of BCP Films. Details about the preparation and installation of PDMS pad and CZA-SS processing can be found elsewhere.[25] The PDMS pads of dimensions similar to the film (≈2.5 cm lateral size) were cut out and manually placed onto the BCP films by light pressing with the smooth surface of the PDMS pad facing the BCP film that allowed for conformal contact with the film during the CZA-SS processing. The BCP samples with the PDMS pad were then translated across the CZA-SS gradient assembly at a speed of 5 μm/s using a syringe pump. The CZA-SS procedure was performed under ambient conditions at different translational velocities. A translation velocity of 5 μm/s corresponds to a T_g to T_g annealing time of about

https://dx.doi.org/10.1021/acsapm.0c00127
ACS Appl. Polym. Mater. 2020, 2, 3072−3083

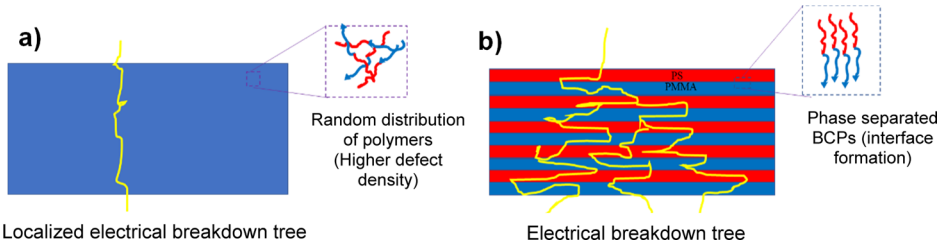

Figure 1. Schematic representation of (a) laterally localized breakdown tree in a homogenous film and (b) tortuous breakdown pathways in multilayered self-assembled block copolymer films.

20 min on the gradient. On the other hand, a slower speed (0.5 μm/s) was used for the higher molecular weight as well as the blend films, in order to expose the BCP film for sufficient time above T_g (≈200 min).

As the film enters the gradient zone above T_g, both the film and the PDMS expand because of the increasing temperature. The coefficient of linear thermal expansion of PDMS ($\alpha_{PDMS} \approx 325 \times 10^{-6}$/°C) is about 4 times that of the underlying BCP ($\alpha_{PS} \approx 80 \times 10^{-6}$/°C, $\alpha_{PMMA} \approx 50 \times 10^{-6}$/°C). This results in differential expansion of the PDMS over the BCP film on the heating side of the gradient and a similar differential contraction on the cooling side. Because of this differential expansion−contraction of the PDMS, single oscillatory shear stress is applied to the BCP film. Based on the expansion induced strain and modulus of the PDMS pad (≈0.4 MPa), the shear stress was calculated to be about 120 kPa. A combination of thermally induced mobility and PDMS induced shear stress directs the alignment of the BCP lamellae parallel to the substrate.

Structural Characterization. *Cross-Sectional Transmission Electron Microscopy.* To image the internal structure of the thin films on Al−quartz substrates, cross sections of the samples were obtained using the FIB lift-out technique. The FIB experiments were performed in collaboration with the Center for Functional Nanomaterials (CFN) at Brookhaven National Laboratory. The cross sections were then imaged using a JEOL 1400 LAB6 transmission electron microscope at 120 keV operating voltage. All images collected were bright-field images.

Neutron Reflectivity. The NR experiments were conducted at the NG7 horizontal reflectometer at the Center for Neutron Research at the National Institute of Standards and Technology (NIST CNR), Gaithersburg, MD. A 4.76 Å collimated neutron beam with a wavelength divergence of 0.18 Å was used. The angular divergence of the beam was varied through the reflectivity scan, and this provided a relative q resolution dq/q of 0.04, where $q = 4\pi \sin(\theta)/\lambda$, and θ is the incident angle with respect to the surface of the film and λ is the wavelength of the beam. Scans were made on BCP films over a wave vector magnitude (q) range from 0.005 to 0.16 Å^{-1}. A pure quartz substrate was used in place of Al-coated quartz for the NR measurements for ease of data fitting. Data fitting and conversion of the NR spectra to the scattering length density and concentration profile were done using the Reflpak software (NIST CNR).

Grazing-Incidence Small-Angle X-ray Scattering Measurement. Grazing-incidence small-angle X-ray scattering (GISAXS) experiments were performed on BCP films in order to investigate the orientation and long-range ordering within the films under different processing conditions for all BCP systems. GISAXS experiments were performed on the beamline 8-ID-E[35] of the Advanced Photon Source, Argonne National Laboratory. An X-ray beam of energy 10.82 keV (8-ID-E) was impinged on the films (in vacuum) at an angle (0.16°) well above the critical angle of the films (0.115°), to probe the bulk of the film. The detector was positioned at a distance of 2185 mm from the sample. Data were collected on a Dectris Pilatus 1M pixel-array detector. Data analysis and conversion to q-space were done using GIXSGUI[36] software in MATLAB, developed at beamline 8-ID-E.

Dielectric Breakdown Testing. The schematic of the experimental setup for performing dielectric breakdown testing can be found in a previous communication.[11] Prior to performing dielectric breakdown measurements, all processed samples were annealed at 80 °C for 12 h to remove residual solvent and adsorbed moisture that may be present within the processed film. Dielectric breakdown trials were performed using a 10 kV Spellman SL300 high voltage supply controlled by a ramping circuit. The ramp was set such that a breakdown event occurs at ≈20 s, in accordance to ASTM standard protocol for short-term dielectric strength tests (which corresponds to 50−300 V/s, depending on the sample).[26] Once >1 mA current passed through the device, a silicon rectifier switch activates and breaks the circuit. The breakdown voltages were read from a Fluke 289 multimeter set in peak capture mode.

The experimental geometry features a copper rod with a hemispherical end (radius of curvature = 2.5 mm) that makes direct contact with the BCP film. The breakdown is confined to a small sample region (area ≈ 0.1 cm^2) in an attempt to remove the influence of film heterogeneity by spatially localizing the electric field. At least 15 breakdown trials were performed for each film to conduct Weibull failure analysis. The copper contact rod was polished after every 15 breakdowns using a diamond paste to remove pitting. A free-standing BOPP film was periodically employed as a test standard to ensure that our experimental platform remained calibrated. All measurements were conducted at room temperature in an N_2 purged environment where relative humidity was observed in the range of 10−20%. Breakdown voltages were converted to breakdown strength by measuring film thickness near each test site via profilometry.

RESULTS

In our recent communication,[11] we demonstrated the effects of different processing methods on the ordering degree of L-BCP morphology and its consequential effects on the overall breakdown and dielectric properties of the film. The as-cast film showed no order and essentially resembled a single-phase homogenous film. Short-term oven annealing led to a perpendicular lamellar morphology while long-term oven annealing led to mixed orientations of the lamellae. A soft-shear DSA method, CZA-SS, demonstrated excellent control over microdomain orientation and led to extremely well-ordered and highly oriented multilayered parallel-to-substrate (aluminum) lamellar structures. Directing the self-assembly of L-BCP films to form a highly ordered multilayered structure parallel to the substrate yielded a commendable increase in the breakdown strength (∼50%) of the L-BCP film, as compared to the unordered as-cast films. The increase in E_{BD} was attributed to the multilayered barrier structure consisting of numerous parallel interfaces by the alternating blocks (dielectrics) of the film. These E-field normal interfaces act as impediments to forestall the breakdown propagation by providing a tortuous path for electrical tree propagation. In fact, when the lamellar domains (layers) of the L-BCP were aligned perpendicular to the electrode, that is, in the direction of the applied field, it resulted in very low breakdown strength values, even lower than that of the as-cast films. Figure 1 is a schematic representation of BCP films with the lamellae aligned normal to the electric field and multiple interfacial barriers forestalling electrical treeing propagation during the

https://dx.doi.org/10.1021/acsapm.0c00127
ACS Appl. Polym. Mater. 2020, 2, 3072−3083

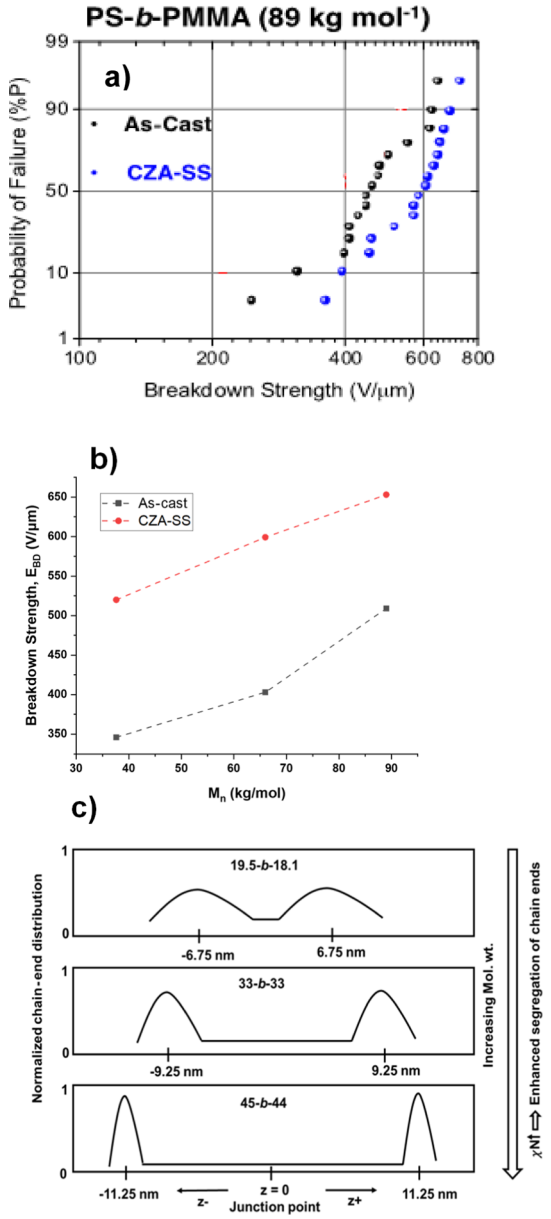

Figure 2. Probability of failure for (a) 45-*b*-44 kg/mol and (b) breakdown strength as a function of molecular weight of neat as-cast and CZA-SS-processed PS-*b*-PMMA films, with lower M_w data taken from ref 11. (c) Schematics of normalized chain-end distribution as a function of molecular weight (adapted with permission from ref 31 Copyright 1993 American Chemical Society).

Table 1. Summary of Characteristic Dielectric Breakdown Strength (E_{BD}) and Shape Parameter β Measured for 19.5-*b*-18.1, 33-*b*-33, and 45-*b*-44 kg mol^{-1} PS-*b*-PMMA Films

sample		E_{BD} (V/μm)	B
19.5k-*b*-18.1k	As-cast	346	5.4
	CZA-SS	520	4.6
33k-*b*-33k	As-cast	403	5.8
	CZA-SS	599	6.1
45k-*b*-44k	As-cast	509	4.5
	CZA-SS	653	5.5

breakdown. The observations from our recent communication[11] highlight the sensitivity of the breakdown phenomenon to the internal L-BCP morphology and orientation. It focused on the role of the L-BCP microstructure in impeding the breakdown propagation as compared to homopolymer control films.

In this work, we decipher the fundamental molecular chain mechanisms by which ordered L-BCPs act to enhance E_{BD} with increasing molecular weight of the L-BCP within the framework of density and distribution of chain ends, interface formation, and layer thickness and compare it to ternary L-BCP blend films swollen by respective homopolymers. Notably, ordered BCPs have well-segregated chain-end distribution, compared to as-cast films that have a random distribution. We investigate these effects on the breakdown strength, E_{BD}, in significantly high M_n neat BCP systems that are nontrivial to order into parallel lamellae using CZA-SS. We focus on the layer thickness (d) and molecular weight dependence of E_{BD} in neat L-BCP films and aim to decouple the effects of individual block layer thickness versus overall chain-end density, by comparing E_{BD} of homopolymer swollen L-BCP films to neat L-BCP films with same layer spacing, d values. In neat L-BCP films, layer thickness d increases with increasing M_n with a simultaneous decrease of chain-end density both of which drive enhanced E_{BD}. However, in ternary blend L-BCP systems, increased layer thickness with added homopolymer drives to increase E_{BD}, but this is countered by increasing chain-end density from added homopolymer to result in a mild increase of E_{BD} with added homopolymer at high concentrations.

A two-parameter Weibull cumulative probability function was employed to fit the breakdown data and is given by $P(E) = 1 - \exp[-(E/E_{BD})^{\beta}]$, where $P(E)$ is the cumulative probability for failure, E is experimental breakdown strength, E_{BD} reflects the electric field where there is 63.2% probability for failure, and β is the shape parameter associated with the least-squares fit of the distribution. Data from these Weibull fits for the as-cast, CZA-SS BCP films with increasing M_n are summarized below in Figure 2a and Table 1.

Effect of Molecular Weight on the Breakdown Strength of L-BCPs. Figure 2 shows the relative comparison of breakdown data and analyses of as-cast versus CZA-SS annealed L-BCP film for varying molecular weights. Figure 2b shows that E_{BD} increases significantly with an almost linear dependence on M_n over as-cast unordered films. The increase of E_{BD} with M_n of as-cast L-BCP films can be understood by comparing them to E_{BD} of homopolymer films that behave similarly, and the results are understood in terms of decreasing chain-end density that are homogeneously distributed in the film. For a homogeneous system of chain-end distribution, such as cast L-BCP films, in the free volume theory of electronic breakdown proposed by Artbauer,[8] it was postulated that under applied fields, electrons gain energy and are accelerated within the molecular voids (defects) or the free volume within the material. The accelerated electrons collide with other electrons transferring energy, leading to a cascading process of breakdown. The higher the free volume, the higher the energy gained by electrons and the greater the number of collisions. In polymers, the chain ends are known to contribute a high fraction toward the net free volume of the film, which explains the linear dependence of E_{BD} on the M_n. For as-cast L-BCP films, the chain-end densities (ρ_c) were calculated using $\rho_c = 2 \times \rho \times N_A/M_n$, where ρ is polymer density, N_A is Avogadro's number, and M_n is the molecular weight of the polymer. Essentially, chain ends can potentially act as defect

https://dx.doi.org/10.1021/acsapm.0c00127
ACS Appl. Polym. Mater. 2020, 2, 3072−3083

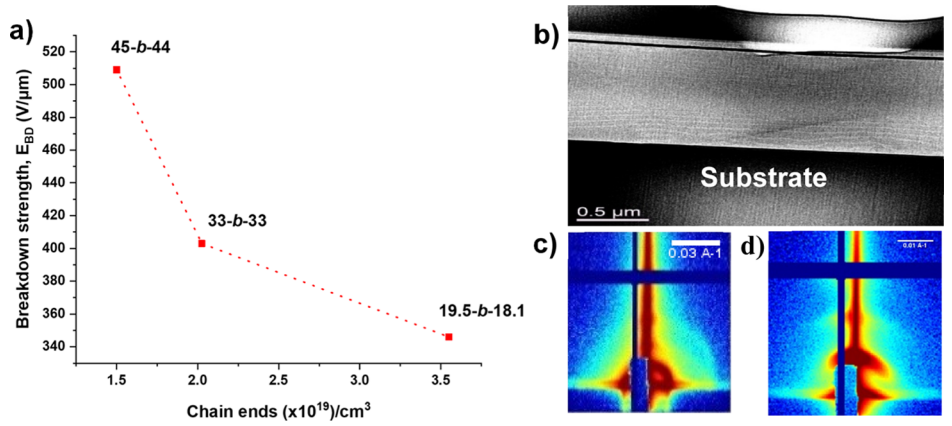

Figure 3. (a) Breakdown strengths of as-cast 19.5-*b*-18.1 kg/mol, 33-*b*-33 kg/mol, and 45-*b*-44 kg/mol PS-*b*-PMMA films as a function of chain-end density (ρ_c) of each system, (b) cross-sectional TEM image of the morphology of neat 45-*b*-44 kg/mol BCP, (c) GISAXS image of 45-*b*-44 kg/mol PS-*b*-PMMA showing ring indicative of isotropic ordering, and (d) GISAXS image of 19.5-*b*-18.1 kg/mol PS-*b*-PMMA showing parallel peaks and no isotropic ring.

Table 2. Summary of Domain Sizes, Layer Thicknesses, and the Number of Layers for CZA-SS-Processed Neat and Blend Films of PS-*b*-PMMA with Varying Homopolymer Concentration

sample	domain size (nm)	layer thickness (nm)	number of layers
neat PS-*b*-PMMA (19.5-*b*-18.1 kg mol^{-1})	27	13.5	≈74
PS-*b*-PMMA + 20% φ_H	38	19	≈53
PS-*b*-PMMA + 40% φ_H	43.3	21.65	≈46
PS-*b*-PMMA + 60% φ_H	46.5	23.25	≈43

sites that initiate or accelerate the breakdown in polymers. Therefore, we conclude that the increased E_{BD} is simply a result of reduced chain-end density with increasing molecular weight, as shown in Figure 3a. Undoubtedly, there are subtleties with respect to the precise component of the breakdown mean-free path, in the thickness (z-) direction of the breakdown pathway that we leave for a future study.

DSA using CZA-SS induces a high degree of parallel ordered lamellae with alternating blocks or layers within the L-BCP films having a definite layer thickness that is defined by the interaction parameter between the blocks (χ) and their molecular weight. For the same molecular weight, the CZA-SS films consistently show higher E_{BD} than the as-cast counterparts despite the same overall chain-end density. For all the molecular weight BCP systems, we observed that CZA-SS-processed films showed a nearly constant and substantial improvement in breakdown strength over the as-cast film on the order of ∼200 V/μm in absolute value to reach a maximum of ∼653 V/μm for the highest M_n (45k-*b*-44k) L-BCP sample. To first order, we interpret this as due to interface and layer formation and well segregated chain-end regimes. Figure 2d illustrates normalized chain-end distribution in an L-BCP film, which is defined as the probability of finding a chain end in unit reference volume along the z-direction.[31]

The CZA-SS-processed L-BCP systems with highest degree of chain-end segregation occur in the L-BCP with the highest

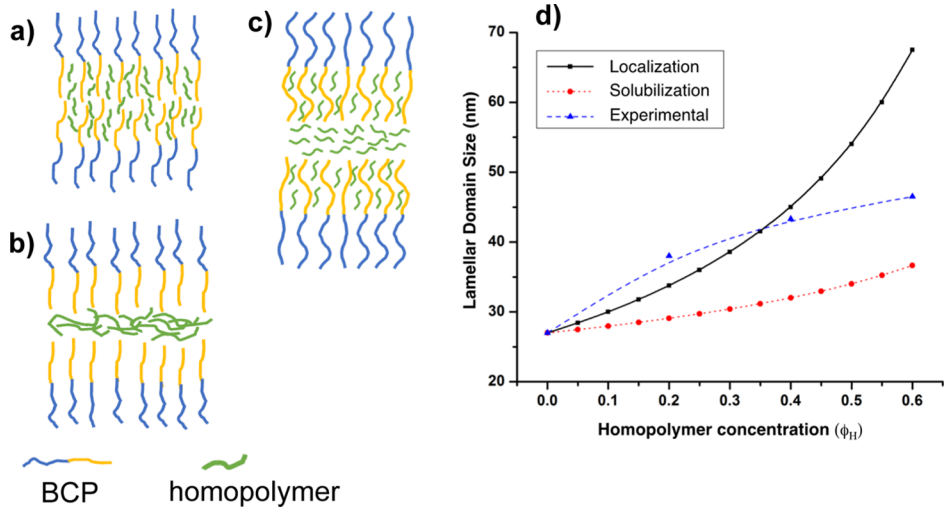

Figure 4. Plot showing (a) solubilization schematic, (b) localization schematic, (c) a combination of localization and solubilization, and (d) lamellar domain size as a function of homopolymer concentration in ternary blend films of PS-*b*-PMMA (19.5-*b*-18.1 kg mol^{-1}) under different conditions of homopolymer segregation within the blocks. A combination (weighted sum) of solubilization (red line value) and localization (black line value) would potentially be most applicable to the experimental data shown at Φ_H = 0.2, reflective of schematic (c) case. The lines are drawn as a guide to the eyes.

https://dx.doi.org/10.1021/acsapm.0c00127
ACS Appl. Polym. Mater. 2020, 2, 3072−3083

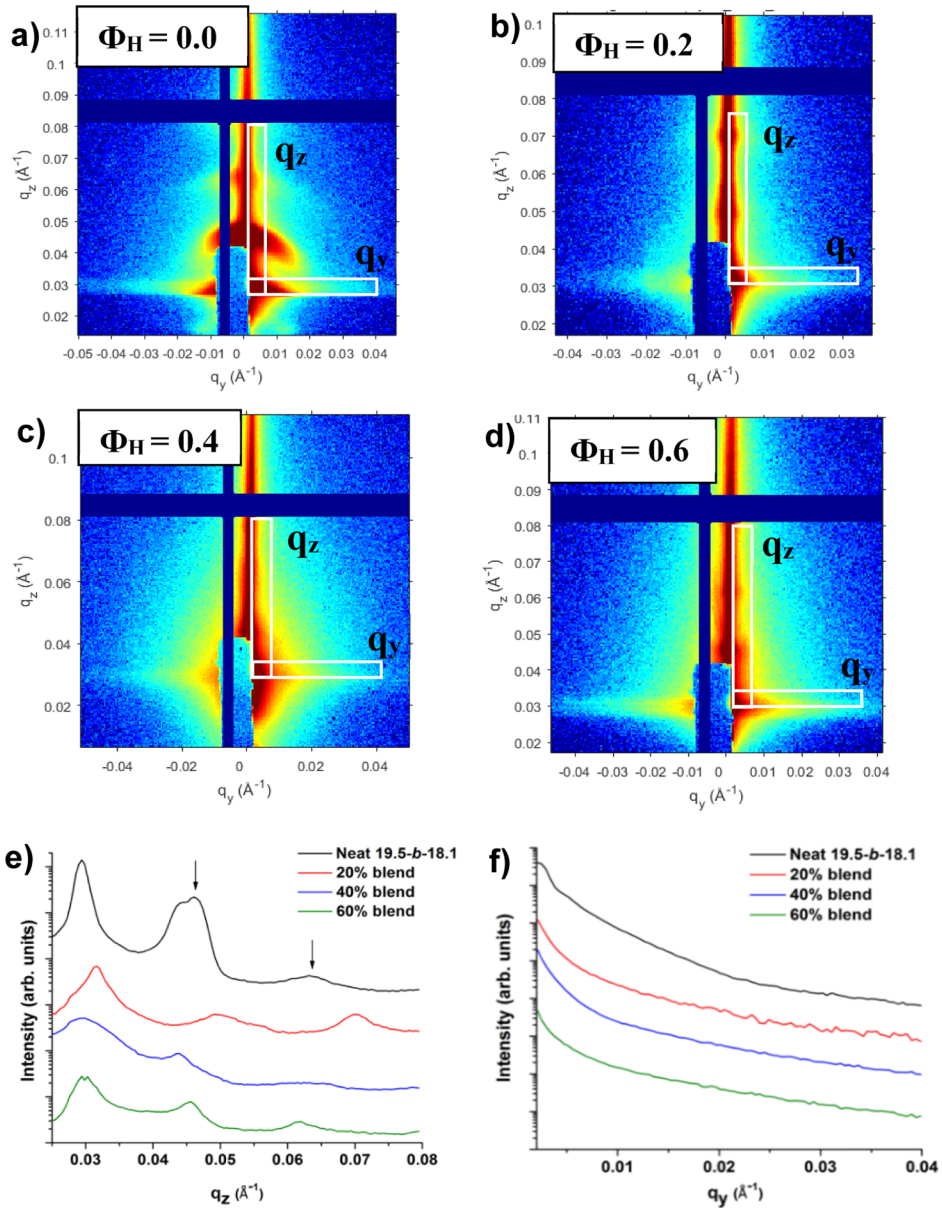

Figure 5. Probing the ordering and orientation of BCP films using GISAXS. Two-dimensional GISAXS images of (a) neat, (b) 20% blend, (c) 40% blend, and (d) 60% blend CZA-SS-processed films with corresponding (e) in-plane and (f) out-of-plane integrated intensity profiles for PS-*b*-PMMA (19.5-*b*-18.1 kg mol^{-1}). Peaks along q_z indicate a morphology with well-defined lamellar domains oriented parallel to the substrate for all the blend systems.

M_n that also exhibits the highest E_{BD}. This may be due to maximal interfacial localization of chain ends in higher molecular weight L-BCP as predicted in simulations.[31] An important factor contributing to the amount of improvement in the E_{BD} is the extent of parallel lamellae alignment in processed films. The CZA-SS-processed high molecular weight (45k-*b*-44k) L-BCP films showed a lesser degree of parallel alignment by GISAXS and cross-sectional transmission electron microscopy (TEM) images (Figure 3b,c) resulting in only ∼30% enhancement in E_{BD}, whereas similarly processed low and moderate molecular weight L-BCP film showed nearly 100% parallel morphology with a ∼50% E_{BD} enhancement (Figure 3d). Because of higher viscosity (lower chain mobility) of high molecular weight PS-*b*-PMMA, the orientation induced by the high surface energy substrate[27,28] and shear induced by the low surface energy PDMS pad at the air surface does not propagate throughout the entire film. Future studies will investigate how to obtain 100% ordered parallel lamellae, possibly with higher temperatures (T_{max}) and lower translational velocity in CZA-SS.

Like the as-cast films, we see a linear increase of E_{BD} in CZA-SS-processed films with molecular weight. However, as mentioned earlier for layered L-BCP films, an increase in M_n is accompanied by an increase in the layer thickness (d); thus, apart from a simple chain-end density model, there could be multiple factors affecting the breakdown including enhanced chain-end segregation, PS-*b*-PMMA junction interfacial effects, and higher layer thickness for the high M_n films. As shown in Figure 2d the chain ends are distributed more uniformly in low molecular BCPs because of lower χN. On increasing the molecular weight, χN increases and chain ends are segregated to interfacial regions as confirmed by SCFT simulations.[31]

https://dx.doi.org/10.1021/acsapm.0c00127
ACS Appl. Polym. Mater. 2020, 2, 3072−3083

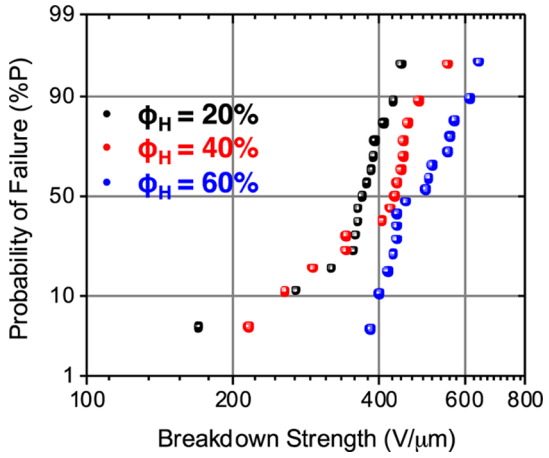

Figure 6. Probability of failure for CZA-SS-processed multilayered ternary blend films of PS-*b*-PMMA (19.5-*b*-18.1 kg mol^{-1}), PS (14 kg mol^{-1}), and PMMA (16 kg mol^{-1}) with total homopolymer concentrations of 20% (black), 40% (red), and 60% (blue).

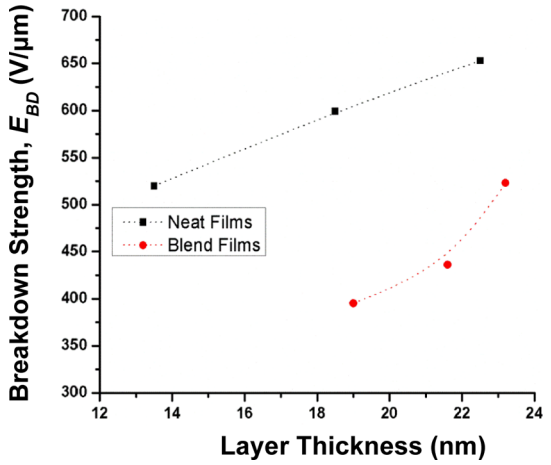

Figure 7. Breakdown strength as a function of increased layer thickness for neat 19.5-*b*-18.1 kg/mol, 33-*b*-33 kg/mol, and 45-*b*-44 kg/mol PS-*b*-PMMA films ordered by CZA-SS and blend films with 20%, 40%, and 60% homopolymer contents.

The junction point fluctuations are decreased by 6% in 33-*b*-33k and by 9% in 45-*b*-44k as compared to 19.5-*b*-18.1k.[37,38] This decrease in the normalized chain-end density with simultaneous enhanced chain-end segregation/localization with increasing M_n in L-BCP films could explain the improvement in E_{BD}.

In terms of the layer thickness effect, Zhou and co-workers found that multilayered coextruded PVDF/polysulfone (PSF) films showed higher electrical conductivity and lower breakdown strengths with decreasing thickness of PVDF and PSF layers.[18] On coextruded multilayered PC/coPVDF films, they found that an optimal layer thickness of ≈160 nm corresponding to about 65 layers in a 10 μm film gave the highest dielectric lifetime under a breakdown field of 320 kV/mm.[19] For L-BCP, because a direct relation exists between the layer thickness (d) and the molecular weight of L-BCP, elucidating the role of layer thickness individually on dielectric properties of L-BCP system for a fixed molecular weight is difficult. To delineate the molecular weight versus layer thickness effect on the breakdown, we kept the molecular weight of the L-BCP system fixed and varied the thickness of the layers by the addition of homopolymers that match the L-BCP blocks, allowing for symmetric swelling of the L-BCP domains. We ensured symmetric PMMA and PS layer thickness in the film by preparing a ternary blend with an equal concentration of PS and PMMA homopolymers in PS-*b*-PMMA. To establish that the addition of homopolymer did not distort the parallel lamellar morphology achieved in CZA processed film, we characterized the morphology of the ternary blend films over macroscopic dimensions using a combination of X-ray (GISAXS) and NR methods. The molecular weight of the L-BCP chosen for the ternary blend was 19.5k-*b*-18.1k (PS-*b*-PMMA) because it showed nearly 100% parallel morphology by soft shear CZA-SS, and the addition of homopolymer can change layer spacing to equivalent thickness of higher M_n neat L-BCPs.

The NR profiles for the neat and blend films of PS-*b*-PMMA after CZA-SS processing are plotted in Figure S1. All films show well-defined five orders of Bragg reflection peaks in q_z corresponding to a high degree of parallel lamellar ordering within the films. A striking feature of the reflectivity profiles is the q_z shift of the Bragg peak positions with increasing homopolymer concentration. The shift in the peak positions by arrows is clearly illustrated in the inset of Figure S1. Additionally, the peaks become narrower on the addition of homopolymers, which indicates that the structural order improves with adding low M_n homopolymers.

For NR, the spacings of the peaks in the reciprocal space, Δq_z, corresponds to the real-space domain size (L_0) by the following equation

$$L_0 = \frac{2\pi}{\Delta q_z} \tag{5}$$

From the peak positions in the reflectivity profiles, the average domain size of L-BCP in the blend films and the corresponding layer thickness were calculated and summarized in Table 2. Next, we compared the domain sizes of L-BCP in blend films with theoretical values. We theoretically determined the lamellar domain sizes as a function of homopolymer concentration in ternary blend films of PS-*b*-PMMA (19.5-*b*-18.1 kg mol^{-1}) under different conditions of homopolymer segregation within the blocks, namely solubilization (eq 3) as shown in Figure 4a compared to localization (eq 4) of the homopolymer as shown in Figure 4b.

Table 3. Summary of the Layer Thickness, Number of Layers, and Corresponding Breakdown Strengths (E_{BD}) for CZA-SS-Processed Multilayered PS-*b*-PMMA Films of Varying Molecular Weights and PS-*b*-PMMA/PS/PMMA Ternary Blend Films

molecular weight films				blend films			
sample	layer thickness (nm)	no. of layers	E_{BD} (V/μm)	sample	layer thickness (nm)	no. of layers	E_{BD} (V/μm)
37.6 kg mol^{-1}	13.5	74	520	φ_H = 20%	19	53	395
66 kg mol^{-1}	18.5	54	599	φ_H = 40%	21.65	46	436
89 kg mol^{-1}	22.5	44	653	φ_H = 60%	23.25	43	523

https://dx.doi.org/10.1021/acsapm.0c00127
ACS Appl. Polym. Mater. 2020, 2, 3072−3083

The solubilization of homopolymers in the L-BCPs refers to the swelling of L-BCP layers by the homopolymer without forming any layering-like localized interphase region between the block.

The localization on the other hand refers to the layering of the homopolymer between the blocks. Solubilization happens when the molecular weight of the homopolymer is much smaller as compared to the BCP, whereas the localization happens when the molecular weight of the homopolymer is comparable or larger as compared to the BCP. However, a combination of solubilization and layering is possible at high concentrations of a low M_n homopolymer, wherein the L-BCP brush layer is saturated with homopolymers in the solubilization limit and excess homopolymer forms a localization interphase layer. Figure 4d shows the lamellar domain sizes of ternary blend films as determined experimentally and theoretically for solubilization and localization cases. Experimentally, strong domain size variation occurs (illustration Figure 4c), wherein the L-BCP brush layer saturates, and localized interfacial segregation layer forms with increasing homopolymer concentration that increases overall layer spacing and thereby E_{BD}, but only modestly, as the added homopolymers also increase the overall chain-end fraction, that counters increase of E_{BD}. This also occurs at modest homopolymer concentration, est. $\Phi_H \sim 0.2$, because the added homopolymer M_n was not much lower, but rather comparable to L-BCP block M_n. Much higher M_n homopolymer addition was avoided for mobility issues that would have resulted in Figure 4b.

The experimental domain sizes agree well with the theoretical values obtained from eq 4 up to 40% homopolymer addition, indicating that the added PS and PMMA homopolymers indeed localize to their respective domains (ideally the center), thereby increasing the domain size (Figure 4b). However, when the homopolymer loading was 60%, the experimental curve did not match either localization or complete solubilization curves, rather showed a domain size in-between the expected theoretical curves for these scenarios. This could be attributed to partial localization and partial solubilization of homopolymers at the high loading. Nevertheless, the domain sizes increase significantly with the addition of homopolymers and are comparable to the domain sizes of the higher molecular weight BCPs.

To provide additional evidence that the lamellae are highly parallel throughout the film thickness in the blend films and there exists little or no vertical domains (in-plane correlation), we performed GISAXS characterization at an angle of incidence (0.16°) higher than the polymer film critical angle (≈0.115°) to investigate the bulk structure of these films. Two-dimensional GISAXS images and their corresponding intensity profiles for the neat and blend PS-*b*-PMMA (19.5-*b*-18 kg mol^{-1}) systems are shown in Figure 5. Horizontal line cuts along q_y (in the $X-Y$ plane of the scattering geometry) and vertical line cuts along q_z as indicated by the boxed areas in Figure 5a−d indicate in-plane (perpendicular lamellae) and out-of-plane (parallel lamellae) ordering, respectively, as shown in Figure 5e,f.

The neat and blend films exhibit no distinct peaks along q_y, indicating that there is no perpendicular lamellae component in the processed film. On the other hand, the presence of peaks in the q_z plane indicates a morphology with well-defined parallel lamellar domains.[33,34] As shown in Figure 5e, we observe a kink in the second-order peak of the neat 19.5-*b*-18.1 kg/mol and in the first-order peak of the 60% blend sample. We are not sure about the origin of this kink. One possible explanation of this kink could be the peak split from overlapped transmitted and reflected beams of X-ray.

Dielectric Breakdown Results of Blend Films. The Weibull plot of breakdown measurements on blend films is shown in Figure 6 and summarized in Table 3 along with comparisons to the neat PS-*b*-PMMA films with varying molecular weights. A definite trend of increasing breakdown strength with increasing layer thickness was observed for the blend films, irrespective of the decreasing total number of layers. Roughly, ≈32% increase in E_{BD} was recorded for a 60% blend film with an average layer thickness of 23 nm over that of a 20% blend film with an average layer thickness of 19 nm. This suggests that the thickness of each lamellar layer in the multilayered film is an important contributing factor to the breakdown strength. For a given molecular weight, a higher layer thickness resulted in an increase in E_{BD} which is in good agreement with previous studies on multilayered dielectric films.[18,19]

Next, we compared the performance of the blend films with neat films of varying molecular weights. The results in Table 3 suggested that addition of 20% homopolymer content caused a significant drop in E_{BD} of the neat L-BCP film despite an increase in the layer thickness. Also, for the same approximate layer thickness and the total number of layers, the E_{BD} of neat films was much higher (≈40−50%) than that of the blend films (Figure 7). For example, a neat PS-*b*-PMMA (33k-*b*-33k) film with molecular weight 66 kg mol^{-1} having a layer thickness of ≈18.5 nm had an E_{BD} of 599 V/μm, whereas a blend film with 20% homopolymer having a similar layer thickness of ≈19 nm had an E_{BD} of just 395 V/μm. Likewise, a neat PS-*b*-PMMA (45k-*b*-44k) film with molecular weight 89 kg mol^{-1} having a layer thickness of ≈22.5 nm and number of layers 44 had an E_{BD} of 653 V/μm, whereas a ternary blend film with 60% homopolymer having layer thickness of ≈23.25 nm and 43 layers had an E_{BD} of only 523 V/μm. These results indicate that the breakdown strength of low molecular weight ternary blend films is not comparable to that of neat high molecular weight L-BCP films for similar layer thickness, suggesting a more significant role of molecular weight of L-BCP on overall dielectric performance. These observations can be rationalized based on the chain end density, homopolymer distribution, and layer thickness of the films. For matched layer thickness and the total number of layers, ternary blend films have a significantly higher number of polymer chains compared to the high molecular weight neat BCP system. As discussed previously, the chain ends can act as defect sites for breakdown because of free volume contribution, according to the free volume theory of dielectric breakdown.[8] The role of chain ends was further validated when we compared the breakdown strength of blend films with 60% homopolymer (523 V/μm) content having almost double the layer thickness (23.25 nm) as that of neat PS-*b*-PMMA (19.5k-*b*-18.1k) films (520 V/μm).

DISCUSSION

Given our recent findings that L-BCP films demonstrating parallel lamellar morphology displayed significantly higher breakdown strengths than their as-cast counterparts, we explored the origins of layer (domain) thickness and molecular weight of the L-BCP on the breakdown strength within the framework of density and distribution of chain ends—one of

https://dx.doi.org/10.1021/acsapm.0c00127
ACS Appl. Polym. Mater. 2020, 2, 3072−3083

the primary factors for breakdown initiation and propagation. For a given BCP, the alignment and ordering of the BCP chains in lamellar microdomains obtained by CZA-SS processing results in a significantly enhanced E_{BD} because of nonhomogenous segregation and localization of chain ends, interface formation, and layer thickness establishment, as compared to the random homogenous distribution in as-cast films. A strong linear correlation was noticed between the molecular weight of the L-BCP system and the overall breakdown performance. E_{BD} was the highest for the highest molecular weight BCP system, despite its limited parallel morphology in the CZA-SS-processed thin film, at the same temperature and thermal gradient conditions as used for all the molecular weight L-BCPs studied. We hypothesize an increase in molecular weight enhances the chain-end segregation to interfacial regions, thereby increasing the probable distance between chain ends which act as defect sites for the dielectric breakdown. In a sense, the mean-free-path for electrical breakdown between homogeneously distributed chain ends in unordered films is much lower than when they are bunched in stratified state in ordered L-BCPs (with high dielectric strength polymer in-between).

To decouple these effects, the molecular weight of L-BCP system was kept constant and the layer thickness and number of layers of the lamellar structure were varied by the symmetric addition of PS and PMMA block component homopolymers to swell the PS-*b*-PMMA L-BCP domains. We infer ternary blends exhibited significantly lower breakdown strength because of homopolymer chain ends that act as breakdown defect sites. The NR data of these ternary blends were used to calculate the domain spacing and to establish that the added homopolymers indeed swell initially at low concentration and subsequently localize to the center of their respective domain at higher concentration, thereby increasing the domain size. Breakdown strength in ternary blends increases only gradually because of layer spacing increase, held back by the simultaneous increase of overall chain-end density from added homopolymers. The ternary blends retained their parallel lamellar morphology, even at up to 60 wt % homopolymer addition to the L-BCP system, because of our CZA-SS processing conditions and surface pinning effects, so that microemulsion phase, if it exists, is maintained largely as a layered structure.

CONCLUSIONS

In summary, we observe that in general, the increase of total number of chain ends in the film greatly lowers the breakdown strength, whereas the increase of parallel layer spacing and interface formation upon ordering in L-BCP systems greatly increases breakdown strength. Specifically, in ternary homopolymer added to block copolymer systems, these effects counter each other, resulting in a sharp drop, followed by a weak increase of breakdown strength with added homopolymer concentration. Adverse chain-end effects seem to affect breakdown strength more nonlinearly in this regard, compared to layer thickness increase, from added homopolymer.

As-cast unordered L-BCP films show molecular weight dependence of breakdown strength similar to literature established homopolymers film results, wherein increasing molecular mass increases breakdown strength, attributable to the reduction of chain-end density as electrical breakdown defects sites. Neat L-BCP parallel ordered by CZA-SS show significant enhanced breakdown strength that increase nearly linearly with molecular mass. This is attributed to a synergy of several effects: chain-end (breakdown defects sites) segregation and localization in layered strata that form with high-breakdown polymer layers in-between the strata. Aside from chain ends, interface formation around L-BCP junction points likely plays a role, but its contribution was kept fixed in these studies by keeping the PS-*b*-PMMA system invariant since interfacial width depends upon BCP interaction parameter. Increasing layer thickness in L-BCP neat with higher molecular weight, or in ternary blends with homopolymer concentration, resulted in enhancing breakdown strength. Future studies must focus on designing high molecular weight, high χ dielectric BCPs as well as DSA processing strategies to align and order such films. Our results provide guiding principles for molecular design of L-BCP-based dielectric films and have important ramifications for next-generation polymer film capacitors and flexible devices based on block copolymers.[44]

ASSOCIATED CONTENT

Supporting Information

The Supporting Information is available free of charge at https://pubs.acs.org/doi/10.1021/acsapm.0c00127.

NR data showing CZA-SS-processed parallelly ordered homopolymer swollen block copolymer films (PDF)

AUTHOR INFORMATION

Corresponding Author

Alamgir Karim − *Department of Chemical and Biomolecular Engineering, University of Houston, Houston, Texas 77204, United States;* orcid.org/0000-0003-1302-9374; Email: akarim3@central.uh.edu

Authors

Saumil Samant − *Department of Polymer Engineering, University of Akron, Akron, Ohio 44325, United States;* orcid.org/0000-0003-4916-0876

Monali Basutkar − *Department of Polymer Engineering, University of Akron, Akron, Ohio 44325, United States;* orcid.org/0000-0002-5920-2104

Maninderjeet Singh − *Department of Chemical and Biomolecular Engineering, University of Houston, Houston, Texas 77204, United States*

Ali Masud − *Department of Chemical and Biomolecular Engineering, University of Houston, Houston, Texas 77204, United States*

Christopher A. Grabowski − *UES, Inc., Dayton, Ohio 45432, United States*

Kim Kisslinger − *Center for Functional Nanomaterials, Brookhaven National Laboratory, Upton, New York 11973, United States*

Joseph Strzalka − *X-Ray Science Division, Argonne National Laboratory, Argonne, Illinois 60439, United States;* orcid.org/0000-0003-4619-8932

Guangcui Yuan − *NIST Center for Neutron Research, National Institute of Standards and Technology (NIST), Gaithersburg, Maryland 20899, United States*

Sushil Satija − *NIST Center for Neutron Research, National Institute of Standards and Technology (NIST), Gaithersburg, Maryland 20899, United States*

Ikeoluwa Apata − *Department of Chemistry, Howard University, Washington, D.C. 20059, United States*

https://dx.doi.org/10.1021/acsapm.0c00127
ACS Appl. Polym. Mater. 2020, 2, 3072−3083

Dharmaraj Raghavan − *Department of Chemistry, Howard University, Washington, D.C. 20059, United States*
Michael Durstock − *Air Force Research Laboratory, Wright Patterson Air Force Base, Dayton, Ohio 45433, United States*

Complete contact information is available at: https://pubs.acs.org/10.1021/acsapm.0c00127

Notes

The authors declare no competing financial interest.
Certain commercial equipment, instruments, or materials (or suppliers, or software, ...) are identified in this paper to foster understanding. Such identification does not imply recommendation or endorsement by the National Institute of Standards and Technology, nor does it imply that the materials or equipment identified are necessarily the best available for the purpose.

■ ACKNOWLEDGMENTS

The block copolymer ternary blend studies were supported by NSF DMR1901127, whereas the block copolymer ordering and processing was supported by NSF DMR 1905996. The breakdown work was supported by AFOSR under contract no. FA9550-12-1-0306. Research carried out at the Center for Functional Nanomaterials, and the National Synchrotron Light Source, Brookhaven National Laboratory, is supported by the U.S. Department of Energy, Office of Basic Energy Sciences, under Contract no. DE-SC0012704. Research carried out at the Advanced Photon Source is supported by the U.S. Department of Energy (DOE) Office of Science User under Contract no. DE-AC02-06CH11357.

■ REFERENCES

(1) Wang, Q.; Zhu, L. Polymer Nanocomposites for Electrical Energy Storage. *J. Polym. Sci., Part B: Polym. Phys.* **2011**, *49*, 1421−1429.
(2) Tchoul, M. N.; Fillery, S. P.; Koerner, H.; Drummy, L. F.; Oyerokun, F. T.; Mirau, P. A.; Durstock, M. F.; Vaia, R. A. Assemblies of Titanium Dioxide-Polystyrene Hybrid Nanoparticles for Dielectric Applications. *Chem. Mater.* **2010**, *22*, 1749−1759.
(3) Kim, P.; Doss, N. M.; Tillotson, J. P.; Hotchkiss, P. J.; Pan, M.-J.; Marder, S. R.; Li, J.; Calame, J. P.; Perry, J. W. High Energy Density Nanocomposites Based on Surface-Modified BaTiO3 and a Ferroelectric Polymer. *ACS Nano* **2009**, *3*, 2581−2592.
(4) Jung, H. M.; Kang, J.-H.; Yang, S. Y.; Won, J. C.; Kim, Y. S. Barium Titanate Nanoparticles with Diblock Copolymer Shielding Layers for High-Energy Density Nanocomposites. *Chem. Mater.* **2010**, *22*, 450−456.
(5) Arbatti, M.; Shan, X.; Cheng, Z.-Y. Ceramic-Polymer Composites with High Dielectric Constant. *Adv. Mater.* **2007**, *19*, 1369−1372.
(6) Grabowski, C. A.; Koerner, H.; Meth, J. S.; Dang, A.; Hui, C. M.; Matyjaszewski, K.; Bockstaller, M. R.; Durstock, M. F.; Vaia, R. A. Performance of Dielectric Nanocomposites: Matrix-Free, Hairy Nanoparticle Assemblies and Amorphous Polymer-Nanoparticle Blends. *ACS Appl. Mater. Interfaces* **2014**, *6*, 21500−21509.
(7) Ieda, M. Dielectric Breakdown Process of Polymers. *IEEE Trans. Electr. Insul.* **1980**, *EI-15*, 206−224.
(8) Artbauer, J. Electric Strength of Polymers. *J. Phys. D: Appl. Phys.* **1999**, *29*, 446−456.
(9) Vogelsang, R.; Farr, T.; Fröhlich, K. The Effect of Barriers on Electrical Tree Propagation in Composite Insulation Materials. *IEEE Trans. Dielectr. Electr. Insul.* **2006**, *13*, 373−382.
(10) Wolak, M. A.; Wan, A. S.; Shirk, J. S.; Mackey, M.; Hiltner, A.; Baer, E. Imaging the Effect of Dielectric Breakdown in a Multilayered Polymer Film. *J. Appl. Polym. Sci.* **2012**, *123*, 2548−2557.
(11) Samant, S. P.; Grabowski, C. A.; Kisslinger, K.; Yager, K. G.; Yuan, G.; Satija, S. K.; Durstock, M. F.; Raghavan, D.; Karim, A. Directed Self-Assembly of Block Copolymers for High Breakdown Strength Polymer Film Capacitors. *ACS Appl. Mater. Interfaces* **2016**, *8*, 7966−7976.
(12) Ku, C. C.; Liepins, R. *Electrical Properties of Polymers*; MacMillan Publishing Company, 1987.
(13) Fischer, P. H.; Nissen, K. The Short-Time Electric Breakdown Behavior of Polyethylene. *IEEE Trans. Electr. Insul.* **1976**, *EI-11*, 37−40.
(14) Claude, J.; Lu, Y.; Wang, Q. Effect of Molecular Weight on the Dielectric Breakdown Strength of Ferroelectric Poly(vinylidene Fluoride-Chlorotrifluoroethylene)s. *Appl. Phys. Lett.* **2007**, *91*, 212904.
(15) Wolak, M. A.; Pan, M.-J.; Wan, A.; Shirk, J. S.; Mackey, M.; Hiltner, A.; Baer, E.; Flandin, L. Dielectric Response of Structured Multilayered Polymer Films Fabricated by Forced Assembly. *Appl. Phys. Lett.* **2008**, *92*, 113301.
(16) Mackey, M.; Hiltner, A.; Baer, E.; Flandin, L.; Wolak, M. A.; Shirk, J. S. Enhanced Breakdown Strength of Multilayered Films Fabricated by Forced Assembly Microlayer Coextrusion. *J. Phys. D: Appl. Phys.* **2009**, *42*, 175304.
(17) Zhou, Z.; Mackey, M.; Carr, J.; Zhu, L.; Flandin, L.; Baer, E. Multilayered Polycarbonate/poly(vinylidene Fluoride-Co-Hexafluoropropylene) for High Energy Density Capacitors with Enhanced Lifetime. *J. Polym. Sci., Part B: Polym. Phys.* **2012**, *50*, 993.
(18) Tseng, J.-K.; Tang, S.; Zhou, Z.; Mackey, M.; Carr, J. M.; Mu, R.; Flandin, L.; Schuele, D. E.; Baer, E.; Zhu, L. Interfacial Polarization and Layer Thickness Effect on Electrical Insulation in Multilayered Polysulfone/poly(vinylidene Fluoride) Films. *Polymer* **2014**, *55*, 8−14.
(19) Zhou, Z.; Mackey, M.; Yin, K.; Zhu, L.; Schuele, D.; Flandin, L.; Baer, E. Fracture Phenomena in Micro- and Nano-Layered Polycarbonate/poly(vinylidene Fluoride- Co -Hexafluoropropylene) Films under Electric Field for High Energy Density Capacitors. *J. Appl. Polym. Sci.* **2014**, *131*, 39877.
(20) Wolak, M. A.; Wan, A. S.; Shirk, J. S.; Mackey, M.; Hiltner, A.; Baer, E. Imaging the Effect of Dielectric Breakdown in a Multilayered Polymer Film. *J. Appl. Polym. Sci.* **2012**, *123*, 2548−2557.
(21) Zhou, Z. Dielectric Properties of Multilayer Polymer Films for High Energy Density Capacitors & Predicting Long-Term Creep Failure of A Bimodal Polyethylene Pipe from Short-Term Fatigue Tests. Doctoral Dissertation, Case Western University, 2014.
(22) Bates, F. S.; Fredrickson, G. H. Block Copolymer Thermodynamics: Theory and Experiment. *Annu. Rev. Phys. Chem.* **1990**, *41*, 525−557.
(23) Torikai, N.; Takabayashi, N.; Noda, I.; Koizumi, S.; Morii, Y.; Matsushita, Y. Lamellar Domain Spacings of Diblock Copolymer/Homopolymer Blends and Conformations of Block Chains in Their Microdomains. *Macromolecules* **1997**, *30*, 5698−5703.
(24) Orso, K. A.; Green, P. F. Phase Behavior of Thin Film Blends of Block Copolymers and Homopolymers: Changes in Domain Dimensions. *Macromolecules* **1999**, *32*, 1087−1092.
(25) Singh, G.; Yager, K. G.; Berry, B.; Kim, H.-C.; Karim, A. Dynamic Thermal Field-Induced Gradient Soft-Shear for Highly Oriented Block Copolymer Thin Films. *ACS Nano* **2012**, *6*, 10335−10342.
(26) American Society for Testing and Materials. *Annual Book of ASTM Standards*, Philadelphia, PA, USA, 1992, Sec., 4, 04−08.
(27) Anastasiadis, S. H.; Russell, T. P.; Satija, S. K.; Majkrzak, C. F. Neutron Reflectivity Studies of the Surface-Induced Ordering of Diblock Copolymer Films. *Phys. Rev. Lett.* **1989**, *62*, 1852−1855.
(28) Anastasiadis, S. H.; Russell, T. P.; Satija, S. K.; Majkrzak, C. F. The Morphology of Symmetric Diblock Copolymers as Revealed by Neutron Reflectivity. *J. Chem. Phys.* **1990**, *92*, 5677−5691.
(29) Mayes, A. M.; Russell, T. P.; Satija, S. K.; Majkrzak, C. F. Homopolymer Distributions in Ordered Block Copolymers. *Macromolecules* **1992**, *25*, 6523−6531.

(30) Mayes, A. M.; Johnson, R. D.; Russell, T. P.; Smith, S. D.; Satija, S. K.; Majkrzak, C. F. Distributions of Chain Ends and Junction Points in Ordered Block Copolymers. *Macromolecules* **1993**, *26*, 1047−1052.
(31) Shull, K. R.; Mayes, A. M.; Russell, T. P. Segment Distributions in Lamellar Diblock Copolymers. *Macromolecules* **1993**, *26*, 3929−3936.
(32) Ahn, H.; Lee, Y.; Lee, H.; Park, S.; Kim, Y.; Cho, J.; Ryu, D. Y. Microdomain Expansion and Transition Behavior of PS-b-PMMA/PS Homopolymers by SAXS Analysis. *Polymer* **2012**, *53*, 5163−5169.
(33) Choi, S.; Kim, E.; Ahn, H.; Naidu, S.; Lee, Y.; Ryu, D. Y.; Hawker, C. J.; Russell, T. P. Lamellar Microdomain Orientation and Phase Transition of Polystyrene-*b*-Poly (Methyl Methacrylate) Films by Controlled Interfacial Interactions. *Soft Matter* **2012**, *8*, 3463−3469.
(34) Shin, C.; Ahn, H.; Kim, E.; Ryu, D. Y.; Huh, J.; Kim, K.-W.; Russell, T. P. Transition Behavior of Block Copolymer Thin Films on Preferential Surfaces. *Macromolecules* **2008**, *41*, 9140−9145.
(35) Jiang, Z.; Li, X.; Strzalka, J.; Sprung, M.; Sun, T.; Sandy, A. R.; Narayanan, S.; Lee, D. R.; Wang, J. The Dedicated High-Resolution Grazing-Incidence X-Ray Scattering Beamline 8-ID-E at the Advanced Photon Source. *J. Synchrotron Rad.* **2012**, *19*, 627.
(36) Jiang, Z. GIXSGUI: A MATLAB Toolbox for Grazing-Incidence X-ray Scattering Data Visualization and Reduction and, Indexing of Buried Three-Dimensional Periodic Nanostructured Films. *J. Appl. Crystallogr.* **2015**, *48*, 917.
(37) Semenov, A. N. Theory of Block-Copolymer Interfaces in Strong Segregation Limit. *Macromolecules* **1993**, *26*, 6617−6621.
(38) Alig, I.; Floudas, G.; Avgeropoulos, A.; Hadjichristidis, N. Junction Point Fluctuations in Microphase Separated Polystyrene−Polyisoprene−Polystyrene Triblock Copolymer Melts. A Dielectric and Rheological Investigation. *Macromolecules* **1997**, *30*, 5004−5011.
(39) Samant, S.; Strzalka, J.; Yager, K. G.; Kisslinger, K.; Grolman, D.; Basutkar, M.; Salunke, N.; Singh, G.; Berry, B.; Karim, A. Ordering Pathway of Block Copolymers under Dynamic Thermal Gradients Studied by in situ GISAXS. *Macromolecules* **2016**, *49*, 8633−8642.
(40) Basutkar, M. N.; Samant, S.; Strzalka, J.; Yager, K. G.; Singh, G.; Karim, A. Through-Thickness Vertically Ordered Lamellar Block Copolymer Thin Films on Unmodified Quartz with Cold Zone Annealing. *Nano Lett.* **2017**, *17*, 7814−7823.
(41) Basutkar, M. N.; Majewski, P. W.; Doerk, G. S.; Toth, K.; Osuji, C. O.; Karim, A.; Yager, K. G. Aligned Morphologies in Near-Edge Regions of Block Copolymer Thin Films. *Macromolecules* **2019**, *52*, 7224−7233.
(42) Liu, G.; Stoykovich, M. P.; Ji, S.; Stuen, K. O.; Craig, G. S. W.; Nealey, P. F. Phase Behavior and Dimensional Scaling of Symmetric Block Copolymer−Homopolymer Ternary Blends in Thin Films. *Macromolecules* **2009**, *42*, 3063−3072.
(43) Zhou, N.; Lodge, T. P.; Bates, F. S. Influence of Conformational Asymmetry on the Phase Behavior of Ternary Homopolymer/Block Copolymer Blends Around the Bicontinuous Microemulsion Channel. *J. Phys. Chem. B* **2006**, *110*, 3979−3989.
(44) Hayirlioglu, A.; Kulkarni, M.; Singh, G.; Al-Enizi, A. M.; Zvonkina, I.; Karim, A. Block Copolymer Ordering on Elastomeric Substrates of Tunable Surface Energy. *Emergent Mater.* **2019**, *2*, 11−22.

https://dx.doi.org/10.1021/acsapm.0c00127
ACS Appl. Polym. Mater. 2020, 2, 3072−3083